Observation of resonance conductance in a quantum point contact with a tunable channel potential

Chong-Shian Wen, J. H. Hsiao, Kuan-Ting Lin, Tzay-Ming Hong, and J. C. Chen
Department of Physics, National Tsing-Hua University, Hsinchu, Taiwan 30013, Republic of China

T. Ueda and S. Komiyama
Department of Basic Science, University of Tokyo, Komaba, Tokyo 153-8902, Japan
(Received 11 March 2010; revised manuscript received 22 June 2010; published 9 September 2010)

We investigate the resonance conductance of a quantum point contact (QPC), defined in a two-dimensional electron gas of a high-mobility GaAs/AlGaAs heterojunction. The potential profile of the QPC channel can be locally tuned by separately biasing the split gate and a cross gate, electrically isolated on the top of the QPC. The conductance, evolving with the cross-gate voltages exhibits an oscillatory feature superimposed on the quantized plateau in the positive bias voltages and a suppression of the plateau in negative bias voltages. Our investigation suggests that the oscillations on the conductance result from the longitudinal resonance through the channel. The governing parameters of the resonance are the aspect ratio of the channel and the Fermi wavelength of the incident electrons.

DOI: 10.1103/PhysRevB.82.115416 PACS number(s): 73.21.Hb, 73.23.Ad

I. INTRODUCTION

One of the hallmarks of mesoscopic physics is the quantization of the conductance in the ballistic transport of electrons through a narrow constriction between two reservoirs.[1,2] A ballistic constriction known as a quantum point contact (QPC) can be defined by electrostatically squeezing the two-dimensional electron gas (2DEG) of a high mobility heterostructure using a metallic split gate. The two-terminal conductance G exhibits plateaus in units of $2e^2/h$ as a function of the split-gate voltages V_{sg}. The quantization of G results from the adiabatic transmission of the spin-degenerate one-dimensional (1D) subbands, formed in the QPC channel. The width of the channel and the electrostatic potential of the QPC change with V_{sg}; hence, the subband energies alter accordingly. Whenever the bottom of the subband energy crosses the Fermi energy E_F, one of the occupied 1D subbands is depopulated and the conductance jumps by $2e^2/h$, yielding a steplike feature in the G-V_{sg} traces.

The quantization on G is known to be sensitive to the process of how the electrons are injected and emitted through the constricted 1D channel.[3,4] The degree of flatness of the plateau, the precision of the quantized values and the sharpness of the steps are closely related to the detailed shape of the electrostatic potential in the constriction region.[5–13] Numerous theoretical calculations show that the precious plateau persists only for an optimum geometry; otherwise, the step features of G are either smeared out or imposed on an oscillatory structure due to the resonant longitudinal electron states in the constrictions. Experiments have been conducted to explore the nature of the resonances.[3,4,14] However, a detailed comparison of the experiments to the theories is difficult. This is because any unavoidable imperfection, such as the presence of an impurity in the channel, can affect the transmission and cause the resonance feature to be device dependent.[15]

In this paper we study the resonance conductance in a QPC by integrating a cross gate on top of the QPC, as displayed in Fig. 1(a). Biasing the cross gate provides a unique technique to continuously vary the QPC potential in a controlled manner. This approach enables us to investigate the evolution of the resonance conductance on the quantized plateau.

II. EXPERIMENTAL RESULTS AND ANALYSIS

A. Device layout and experimental setup

The devices were fabricated on a GaAs/AlGaAs heterostructure, containing a 2DEG at 80 nm below the surface and with an electron density of $n_s=2.1\times10^{11}$ cm^{-2} and a mobility of $\mu=1.1\times10^6$ cm^2/V s at 4.2 K. The device consists of a split gate and a top cross gate, as schematically displayed in Fig. 1(a). Figure 1(b) shows the scanning electron microscope (SEM) image of the device. A mesa structure is defined by wet etching and all of the metal gates are patterned by electron-beam lithography. The point contacts are formed by applying negative voltages to the split gate. The lithographic channel width and length of the QPC are 300 nm and 310 nm, respectively. A cross gate is electrically isolated from the QPC by a 170-nm-thick overexposed PMMA (Polymethyl methacrylate), which serves as spacer layers to decrease the local capacitance. The cross gate is designed to be located on top of the split gate and transversely across the center of the conducting channel. Thus, the cross gate can be used to fine tune the barrier potential in the channel. The variance of the cross-gate position due to the lithographic alignment error in different devices is about ±10 nm. The experimental results presented in this paper are obtained from three devices. All devices display consistent behaviors, regardless the thermal cycles. The experiment is carried out in a ^{3}He cryostat with a 300 mK base temperature or in a dilution refrigerator with a base temperature of 25 mK. Two-terminal conductance measurement was made by applying a low-frequency ac bias voltage $V_{rms}\leq10$ μV (17 Hz) to the source contact while the drain contact was grounded.

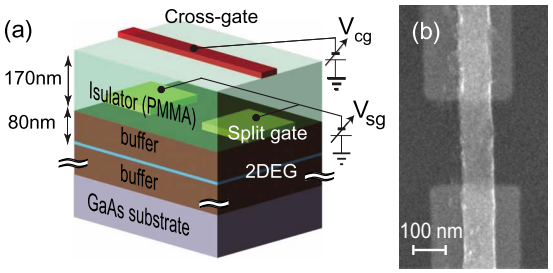

FIG. 1. (Color online) (a) A schematic drawing of the cross-sectional view of the device. (b) An SEM image of the device.

B. Resonant conductance in a quantum point conduct

Figure 2 shows G of Sample 1 as a function of the split-gate voltage V_{sg} and the cross-gate voltage V_{cg} at a temperature $T=0.3$ K and in the absence of the magnetic field, $B=0$ T. The integer plateaus are duly observed. The pinch-off voltages V_p of the split gate on each G-V_{sg} trace vary with V_{cg} and can be expressed as $V_p \sim -0.17 \times V_{cg} - 1.38$ V. The linear dependence of V_p on V_{cg} suggests that V_{cg} affects the confining potential in the QPC channel and changes the carrier density within. Because the cross gate is ~250 nm above the 2DEG and locates further away than the split gate, it can induce a potential modulation much wider than its width.

Close examination of Fig. 2 shows that, as associated with the shift of the plateau positions, the detailed plateau feature gradually evolves with V_{cg}. To clearly reveal the changes in the plateau details, Fig. 3 illustrates the enlarged portions of the last three plateaus in three devices measured. For clarity, here V_{sg} is offset to ΔV_{sg}, so that only the plateau region is displayed. Figures 3(a)–3(c), Figs. 3(d)–3(f), and Figs. 3(g)–3(i) are extracted from Sample 1, Sample 2, and Sample 3, respectively. For comparison, each subfigure of Fig. 3 displays two traces with two representative V_{cg}'s of each sample. The black traces are used for small or positive V_{cg}; in contrast, the red traces are used for more negative V_{cg}.

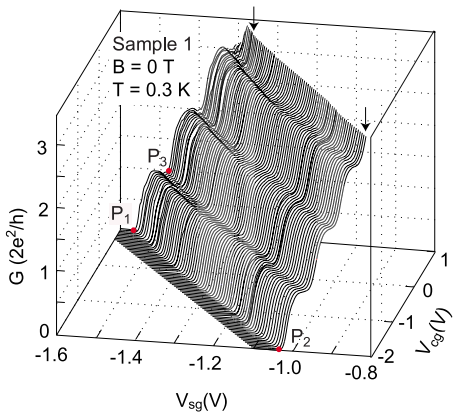

FIG. 2. (Color online) Conductance of Sample 1 as a function of the split-gate voltage V_{sg} and the cross-gate voltage V_{cg}. V_{cg} is scanned from −2 to 1.0 V in steps of 40 mV at $T=0.3$ K. The red points P_1, P_2, and P_3 are marked for the simulation of the channel potential, discussed in Sec. II C. The enlarged plateau features of the traces marked by the arrows are displayed in Figs. 3(a)–3(c).

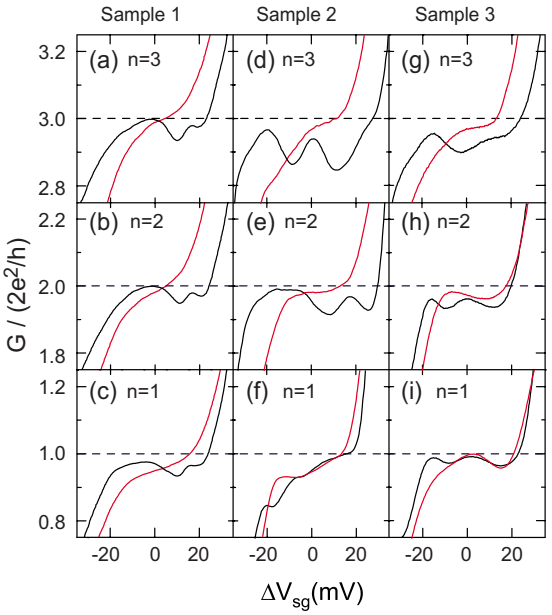

FIG. 3. (Color online) The enlarged last three plateaus of the three samples. (a)–(c) for Sample 1 at $T=0.3$ K, (d)–(f) for Sample 2 at $T=30$ mK, and (g)–(i) for Sample 3 at $T=30$ mK. The black/red curves represent $V_{cg}=0.8$ V/−2 V for Sample 1, 0.0 V/−1.84 V for Sample 2, and −0.6 V/−1.85 V for Sample 3, respectively.

Depending on the polarity and the magnitude of V_{cg}, the plateau develops into different features. When V_{cg} is small, a ripple feature already emerges on the steplike conductance. The oscillatory characteristics become more pronounced for higher-order plateaus or for positive V_{cg}. As the cross gate is more negatively biased, the oscillations on the G steps tends to become less visible or even disappears. The appearance and suppression of oscillatory structures on G associated with different gating conditions are generally found in the three samples. It should be noted that all plateaus are below their ideal quantization values, indicated by the dashed lines in Fig. 3. After subtracting the residue and the contact resistances in series with the QPC, the deviations from the exact quantization are estimated within 6–10 %. The prerequisite for accurate quantization is that the plateaus are flat but the oscillations inhibit the exact quantization.

We now wish to interpret the experimental findings. The appearance of the oscillatory features, as V_{cg} is positive, suggests that biasing the cross gate not only causes a modulation of the carrier density in the channel but also subtly deforms the channel potential. The correlations between the confining potential and the profile of conductance step have been widely studied.[5–13] The potential near the middle of QPC can be approximated by a saddle point with curvatures ω_x and ω_y, where x is the transport direction.[13,16] When ω_y is larger, namely, when the potential profile is steeper, the spacing of energy levels becomes wide, which results in longer plateaus.

For the oscillatory feature, it has been predicted and related to a Ramsauer-type resonance in the transmission,[5,6] i.e., the oscillations are due to the constructive interference between reflected and incoming waves within the QPC chan-

nel. To gain an intuitive view of the physical origin of the oscillations, we note that as noninteracting electrons with energy E in a one-dimensional wire encounter a square-barrier potential of length L and height V_0, the transmission probability $\mathcal{T}$ for $E>V_0$ equals

$$\mathcal{T}=\{1+\sin^2(kL)/[4(E/V_0)(E/V_0-1]\}^{-1},$$

where $kL=L\sqrt{2m_0(E-V_0)/\hbar}$ and m_0 denotes the mass of the charge carriers.[17] G can be described by the Landauer formula, $G=(2e^2/h)\mathcal{T}$.[18] Hence, the sine term of $\mathcal{T}$ causes the oscillations on G when we vary E/V_0.

The oscillations in a QPC can be viewed as the transmission resonates with standing waves in between the edges of both ends of the constrictions, as the boundary condition $k_xL=N\pi$ is satisfied, where k_x is the longitudinal wave vector, L is the channel length, and N is the number of oscillations. If the widening of the constriction changes sufficiently gradual, the transport is adiabatic and the oscillations disappear. More rigorous calculations demonstrate that N is a function of the aspect ratios L/W and Fermi wave vector k_F of the electrons in the channel, where W is the width of the QPC channel.[5,6,11,12] The oscillatory feature is more pronounced for larger L/W or larger k_F.

Ramsauer-type oscillatory features can also be induced by the presence of impurity scattering in a quasi-one-dimensional wire.[15,19] Strictly, it is difficult to completely rule out the interference signal involving the impurity scattering or the device defects in our experiment. However, the distinct oscillatory features on G are reproducible in the three devices. This implies that the observed oscillations and their changes are unlikely dominated by a random disorder scattering process but resulted from a genuine interference phenomenon residing in the channel.

Experimentally, we estimate $L\sim 250$ nm based on the lithographic size of the device and the depletion regions around the split gate. Within the last three plateaus concerned, L can be considered to be almost unchanged. Thus, the number of oscillations on a plateau is proportional to k_x. Upon decreasing W with more negatively biasing V_{sg}, the Fermi level crosses a sequence of 1D subbands. k_x in the threshold of the $(n+1)$th subband decreases from $k_x=(2m^*E_n/\hbar^2)^{1/2}$ to 0, where the nth subband with energy spacing $E_n=\hbar\omega_y$ begins to be depopulated.

To substantiate the above interpretations with our observations, we extract the relevant parameters, L/W and k_F, governing the resonant oscillations. We select the second plateau as an example and evaluate E_2 by applying a magnetic field perpendicular to the QPC to depopulate the magnetoelectric subbands.[3,20] Ignoring spin degeneracy and considering a parabolic confining potential, we can express the number of occupied subbands n as $n=\text{int}[E_F/\hbar\omega+1/2]$, where $\omega=\sqrt{\omega_y^2+\omega_c^2}$ is the hybrid parabolic confinement parameter ω_y and the cyclotron frequency $\omega_c=eB/m^*$. $m^*=0.067m_0$ is the effective mass of electrons. Figure 4 shows the conductance in the presence of the magnetic field for two representative V_{cg} of Sample 2. When the magnetic field is stronger, the plateau width becomes widen, reflecting a larger ω. For a comparison with our data, we adopt the calculations in Ref. 4 and define an effective channel width W_{par} as W_{par}

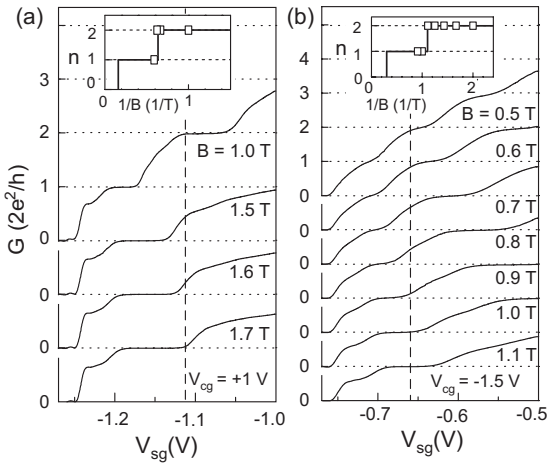

FIG. 4. The conductance G of Sample 2 as function of V_{sg} at several values of the magnetic field at 0.3 K. The curves have been offset for clarity. (a) $V_{cg}=1$ V. (b) $V_{cg}=-1.5$ V. The insets show the number of occupied subbands, n, as a function of the inverse magnetic fields at the fixed V_{sg}, where $V_{sg}=-1.12$ V for (a) and $V_{sg}=-0.66$ V for (b), marked by the dashed lines. The solid lines of the insets are the theoretical curves according to Eq. (1).

$\equiv 2\hbar k_F/m^*\omega_y=n_{1D}/n_s$, where n_{1D} is the number of electrons per unit length in the channel and $n_s=k_F^2/2\pi$ is the 2DEG sheet density. Hence, n can be rewritten as

$$n=\text{int}\left\{\frac{1}{2}+\frac{1}{4}k_FW_{par}[1+(W_{par}/2l_c)^2]^{-1/2}\right\}, \qquad (1)$$

where $l_c\equiv\hbar k_F/eB$. It should note that here we consider k_F of the 2DEG near the QPC and assume k_F is the same as that inside QPC channel. Equation (1) describes that more negatively biasing V_{sg} changes n by reducing both W_{par} and k_F (through the change in n_s). As V_{sg} is fixed, then n can be depopulated by B (through the change in l_c). The insets of Fig. 4 display the corresponding n versus B^{-1} for $V_{sg}=-1.12$ and -0.66 V, chosen where the magnetic depopulation of the second subband is observed. k_F and ω_y can be obtained by the fit of Eq. (1) to the data. k_F, the second subband energy $E_2=\hbar\omega_y$, the derived W_{par}, and n_{1D} are summarized in Table I. The subband spacing E_2 and the ratio L/W_{par} increases with more positive biasing of the cross gate or with more negative biasing the split gate. For larger E_2, great variation in V_{sg} is required to depopulate a new subband and gives more N. The larger L/W_{par} results in stronger

TABLE I. Values of the subband spacing $E_2=\hbar\omega_y$, the Fermi wave vector k_F, the effective width W_{par}, and the channel carrier density n_{1D}.

V_{cg}/V_{sg} (V)	E_2 (meV)	k_F (1/nm)	W_{par} (nm)	n_{1D} (10^6 cm^{-1})
−1.5/−0.62	1.12	0.083	169	1.85
−1.5/−0.66	1.22	0.073	136	1.16
+1.0/−1.05	1.83	0.106	132	2.38
+1.0/−1.12	2.15	0.097	103	1.55

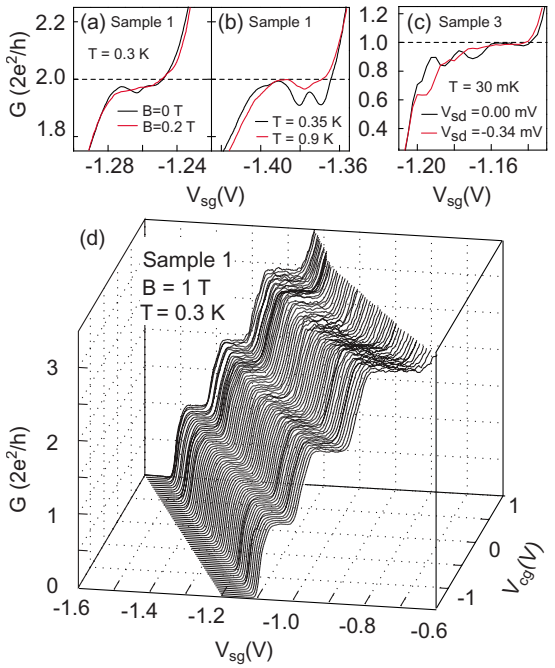

FIG. 5. (Color online) Comparison between conductance plateaus as a function of V_{sg} obtained at: (a) $B=0$ and 0.2 T, with $V_{cg}=0$ V and $T=0.3$ K; (b) $T=0.35$ and 0.9 K, with $V_{cg}=1$ V and $B=0$ T, and (c) $V_{sd}=0$ V and 0.34 mV, with $V_{cg}=0$ V, $T=30$ mK, and $B=0$ T. (d) The conductance is plotted as a function of V_{sg} and V_{cg} at $B=1$ T. The plateaus are longer as V_{cg} is more negatively biased. Fine conductance fluctuations are observed and more pronounced on the third plateau. The data in (a), (b), and (d) were taken from Sample 1 and (c) was taken from Sample 3.

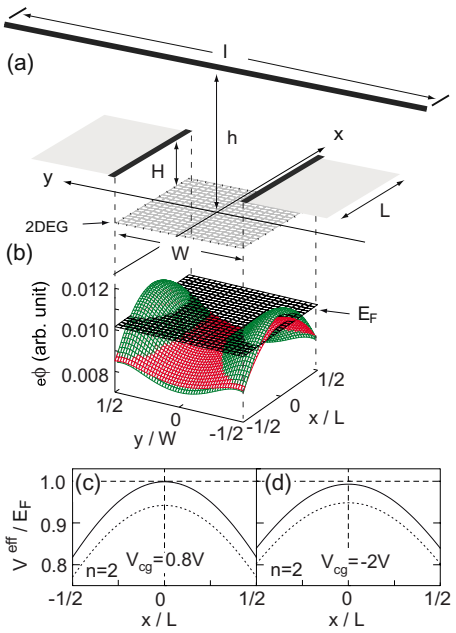

FIG. 6. (Color online) (a) A schematic to illustrate the model for the simulation of the potential profile around the QPC. The electrostatic potential energy $e\phi(x,y)$ modulated by the split and cross gates is calculated by three charged lines represented by the thick black lines. (b) The distribution of potential energy is plotted with the realistic parameters from the experiment: $L=W=3$, $H=0.8$, $l=10$, and $h=2.5$ (all in units of 100 nm). The green and red surfaces representing the $(V_{sg},V_{cg})=(-1.44,0.8)$ V and $(-0.95,-2)$ V, respectively. For (c) and (d), the effective potential energy is plotted as a function of x at $y=0$. Panel (c) is for $V_{cg}=0.8$ V and (d) is for $V_{cg}=-2.0$ V. The bold/dotted curves represent the V_{sg} at the left/right ends of the $n=2$ plateau.

resonance, giving more apparent oscillations, as theories predict.[5,6,11,12] It explains why the oscillatory features are more pronounced as V_{cg} becomes more positive for a given n, as shown in Figs. 2 and 3.

Next we wish to address the evolution of the oscillations in different plateaus at a given V_{cg}. We note that less negative biasing of the split gate not only increases L/W_{par} and E_2 but also reduces k_F. In contrast to larger L/W_{par} and E_2, the smaller k_F is expected to abate the oscillation strength.[5] Therefore, the occurrence of the oscillations depends on the delicate competition between L/W_{par} and k_F. For the black curves shown in Fig. 3, k_F plays a dominant role in the occurrence of the oscillations, compared with the aspect ratio of the channel, so the resonant oscillations are less visible at smaller n. However, for the red curves shown in Fig. 3, these bump features found on the $n=1$ plateau of Sample 2 and $n=1$ and 2 plateaus of Sample 3 may suggest the resurgence of resonance state due to larger L/W_{par}. The overall features of our findings agree well with the theoretically predicted general behaviors of resonance conductance. Our experiments demonstrate the evolution of resonance conductance in a QPC with the governing parameters, L/W and k_F.

C. Temperature, magnetic field, and biasing voltage effects on the resonance conductance

In this section we investigate the rigidity of the resonant states against B, T, and a dc source-drain voltage V_{sd}. As the cyclotron radius is comparable to the characteristic length of the resonant states, i.e., the size of the QPC ($\sim$300 nm), the resonant states can be seriously affected. Figure 5(a) shows that the oscillatory G is washed out at $B\sim0.2$ T, and that the cyclotron radius is $\sim$290 nm. Moreover, the resonance structure can also be smoothed by both thermal and voltage broadening of the conductance.[3,5,6] As an appropriate energy window on the Fermi surface is opened either by thermal broadening or voltage broadening, the quantized energy levels become less important. Consequently, the resonance features tend to be averaged out.[3,21] Figures 5(b) and 5(c) reveal the degradation of the oscillations with elevated $T\sim0.9$ K and increased $V_{sd}\sim0.34$ mV, respectively. The corresponding thermal averaging over an energy window on the order of $4k_BT\sim0.3$ meV consists of the energy range for the voltage broadening eV_{sd}.

A recent theoretical study indicated that for a nanostructure embedded in a quasi-one-dimensional wire under a magnetic field the conductance may either exhibit distinct resonant features on the plateau due to the formation of quasibound states in the vicinity of the attractive scattering center or be suppressed in a repulsive scattering potential.[22] The theoretical calculations of Ref. 22 predicted G can drastically change with the inclusion of a scattering potential under the magnetic field in a range around $B=1$ T. Figure 5(d) shows that G is measured at $B=1$ T. Within the range

of potentials tuned by V_{cg}, G displays a sharper transition between plateaus, and the predicted conductance features are unobservable. The absence of pronounced resonant states at finite B provides indirect evidence that the disorder-related backscattering may be neglected in our devices, and the oscillations observed at $B=0$ T most likely result from a genuine resonance effect.

Conductance fluctuations, predominantly on the third, less on the second and nearly invisible on the first plateau, is found. The fluctuations resemble the universal conductance fluctuations. Since the QPC has a longer channel length and the l_c at $B=1$ T can be less than the channel width at higher n, we speculate that fluctuations may arise from the enhanced specular backscattering at the exit of the constriction or boundary scattering at the channel wall irregularities. The transmission probability decreases with the narrowing of the channel; and, the fluctuation amplitudes are dampened.

D. Numerical model calculations

We have elaborated oscillations on G plateaus in terms of the longitudinal wave resonances based on the ω_y, L/W_{par}, and k_F determined experimentally in Sec. II C. It would be instructive to reveal that the oscillations can indeed occur due to the nature of the electrostatic potential of the QPC in the present device layout. Should the confinement in QPC be simulated by an infinite square wall, its geometry will be crucial to determine the number of oscillation periods occur within the variation in V_{sg} for the plateau.[5,6] Instead of doing such an approximation, we calculate and use the full electrostatic potential of the QPC due to the gate voltages to account for all plateau features. We only study the last three plateaus, where the bottom of the conduction band is left up.

We assume the amount of charge accumulated on the gates to be proportional to the gate voltage, which enables us to obtain a potential profile (shown in Fig. 6). The model used to simulate the potential profile is illustrated in Fig. 6(a), where W denotes the width of the QPC and $L(l)$ and $H(h)$ represent the length and height of the split (cross) gate, respectively. Since the cross gate is far away from the 2DEG plane, we can treat it as a charged line. Equation (2) expresses the electrostatic potential energy $e\phi(x,y)$ seen by electrons in the 2DEG due to the gates alone. Here we assume that the electric effect resulting from the complicated layer structures can be incorporated into the two parameters α and β,[23]

$$\phi(x,y) = -\alpha V_{sg}\left\{\ln\left[\frac{\frac{L}{2}-x+\sqrt{\left[\left(\frac{L}{2}-x\right)^2+\left(\frac{W}{2}+y\right)^2+H^2\right]}}{-\frac{L}{2}-x+\sqrt{\left(\frac{L}{2}+x\right)^2+\left(\frac{W}{2}+y\right)^2+H^2}}\right]+\ln\left[\frac{\frac{L}{2}-x+\sqrt{\left[\left(\frac{L}{2}-x\right)^2+\left(\frac{W}{2}-y\right)^2+H^2\right]}}{-\frac{L}{2}-x+\sqrt{\left(\frac{L}{2}+x\right)^2+\left(\frac{W}{2}-y\right)^2+H^2}}\right]\right\}$$
$$-\beta V_{cg}\ln\left[\frac{\frac{l}{2}+\sqrt{x^2+\frac{l}{2}^2+h^2}}{-\frac{l}{2}+\sqrt{x^2+\frac{l}{2}^2+h^2}}\right]. \quad (2)$$

As an even function of y, Eq. (2) can be reduced to a simple-harmonic potential by Taylor expanding around the QPC position at $y=0$.[13,16] Its corresponding eigenvalues $(n-1/2)\omega_y$ are then used in defining an effective potential energy along the transport x direction,[23]

$$V^{eff}(x) = e\phi(x,y=0) + (n-1/2)\hbar\omega_y(x), \quad (3)$$

where $\omega_y=\sqrt{e\phi''(x,y=0)/m^*}$. Note that in the center of the QPC channel, ω_y can be viewed as proportional to $\sqrt{\alpha|V_{sg}|}$. Strictly, both coefficients α and β in Eq. (2) may vary with V_{cg} and V_{sg}. To simplify, we ignore the small variations and treat them as constants. As the V^{eff} for each n passes through the Fermi surface, i.e., $V^{eff}=E_F$, the conductance experiences the G_n plateaus. Therefore, the magnitudes of coefficients α and β can be estimated by setting them equal to the potential V^{eff} from Eq. (3) at the left ends of the plateaus. As an example, we select three such points marked in Fig. 2, where (V_{sg},V_{cg}) equals $(-1.52,0.8)$ V, $(-1.03,-2.0)$ V, and $(-1.44,0.8)$ V for points P_1 and P_2 at the $n=1$ plateau and P_3 at the $n=2$ plateau, respectively. By setting V^{eff} at P_1 equal to that at P_2, and that at P_1 equal to that at P_3, we obtain $\alpha=2.24\times10^{-3}$ and $\beta=4.44\times10^{-4}$. Figure 6(b) illustrates two curves of $e\phi(x,y)$ for $(V_{sg},V_{cg})=(-1.44,0.8)$ V and $(-0.95,-2)$ V, where E_F is shown for reference.

Next, we discuss the length of the conductance plateaus. Take the green surface corresponding to $V_{cg}>0$ in Fig. 6(b), for instance. The curvature in the y direction of the green surface is larger than the red surface; therefore, a more negative V_{sg} is required for the green surface than for the red surface with a negative V_{cg} to remain at the same plateau. The former case compacts the electronic wave function and widens the energy spacing $\hbar\omega_y$. This implies that a greater variation in V_{sg} is required to reach the next energy level, which renders a longer plateau.[13]

For this work, a detailed distribution of the potential is calculated and is allowed to vary as the gate voltage changes. We count the number of oscillations by using the WKB approximation: $N=\int dx\sqrt{2m^*[E_F-V^{\text{eff}}(x)]}/h$. Figures 6(c) and 6(d) show the profiles of $V^{\text{eff}}(x)$ with the V_{sg} and V_{cg} values that correspond to the beginning and end positions of the plateau, displayed as the dotted and solid lines, respectively. We find that the vertical spacing between these two curves is wider in panel (c), indicating that a wider range of potential energy is required to sweep through the plateau. This consequently allows more oscillations. To compare this with the number of oscillations ΔN observed in the experiments, we can determine ΔN by subtracting the N values obtained at the dotted and solid lines. We estimate that the ratio $\Delta N(V_{cg}=0.8\ \text{V})/\Delta N(V_{cg}=-2\ \text{V})\sim 1.3$ for the $n=2$ plateau. Compared with the oscillations displayed in Fig. 3(c), the calculated ratio agrees well with the experimental observations. Our present model is too simplified to evaluate the exact ΔN. For a more precise analysis, a more sophisticated model and self-consistent calculation must be employed.

III. CONCLUSIONS

We have observed a resonance structure superimposed on the conductance plateau of a QPC with a cross gate electrically isolated on top of the QPC channel. The channel potential of the QPC can be separately tuned by biasing the cross gate and the split gate. Associated with the delicate modulation of the potential profile, the continuous evolution of the conductance plateaus from the suppression of the plateau to the oscillations is observed. By depopulating the subbands in the perpendicular magnetic fields, we determine the subband energy, the Fermi wavelength and the effective potential width of the narrow channel under different gating conditions. Our analysis suggests that the observed oscillatory features originate from longitudinal wave resonances in the channel. The oscillatory behaviors reflect the aspect ratio and the Fermi wavelength of the channels. Finally, we propose a simple model to numerically describe the nature of the resonance behaviors observed in these experiments.

ACKNOWLEDGMENTS

We acknowledge C. C. Chi, A. M. Chang, and Chi-Shung Tang for helpful discussions. J. C. Chen thanks Y. P. Lin for assistance with the experiments. This work is supported by the National Science Council (Grant No. NSC 95-2112-M-007-049-MY3) in Taiwan and the Boost project of the University.

[1] B. J. van Wees, H. van Houten, C. W. J. Beenakker, J. G. Williamson, L. P. Kouwenhoven, D. van der Marel, and C. T. Foxon, Phys. Rev. Lett. **60**, 848 (1988).
[2] D. A. Wharam, T. J. Thornton, R. Newbury, M. Pepper, H. Ahmed, J. E. F. Frost, D. G. Hasko, D. C. Peacock, D. A. Ritchie, and G. A. C. Jones, J. Phys. C **21**, L209 (1988).
[3] B. J. van Wees, L. P. Kouwenhoven, E. M. M. Willems, C. J. P. M. Harmans, J. E. Mooij, H. van Houten, C. W. J. Beenakker, J. G. Williamson, and C. T. Foxon, Phys. Rev. B **43**, 12431 (1991).
[4] C. W. J. Beenakker and H. van Houten, *Solid State Physics* (Academic Press, New York, 1991), Vol. 44, p. 1.
[5] A. Szafer and A. D. Stone, Phys. Rev. Lett. **62**, 300 (1989).
[6] G. Kirczenow, Phys. Rev. B **39**, 10452 (1989).
[7] L. Escapa and N. García, J. Phys.: Condens. Matter **1**, 2125 (1989).
[8] E. Tekman and S. Ciraci, Phys. Rev. B **39**, 8772 (1989).
[9] E. Tekman and S. Ciraci, Phys. Rev. B **40**, 8559 (1989).
[10] S. He and S. Das Sarma, Phys. Rev. B **40**, 3379 (1989).
[11] D. van der Marel and E. G. Haanappel, Phys. Rev. B **39**, 7811 (1989).
[12] Y. Avishai and Y. B. Band, Phys. Rev. B **40**, 12535 (1989).
[13] M. Büttiker, Phys. Rev. B **41**, 7906 (1990).
[14] Q. Wang, N. Carlsson, I. Maximov, P. Omling, L. Samuelson, W. Seifert, W. Sheng, I. Shorubalko, and H. Q. Xu, Appl. Phys. Lett. **76**, 2274 (2000).
[15] J. C. Chen, Y. Lin, K. T. Lin, T. Ueda, and S. Komiyama, Appl. Phys. Lett. **94**, 012105 (2009).
[16] C. K. Wang and K. F. Berggren, Phys. Rev. B **57**, 4552 (1998).
[17] R. Eisberg and R. Resnick, *Quantum Physics* (Wiley, New York, 1974).
[18] H. Bruus and K. Flensburg, *Many-Body Quantum Theory in Condensed Matter Physics* (Oxford University Press, US, 2004).
[19] P. F. Bagwell, Phys. Rev. B **41**, 10354 (1990).
[20] T. P. Martin, C. A. Marlow, L. Samuelson, A. R. Hamilton, H. Linke, and R. P. Taylor, Phys. Rev. B **77**, 155309 (2008).
[21] P. F. Bagwell and T. P. Orlando, Phys. Rev. B **40**, 1456 (1989).
[22] V. Gudmundsson, Y.-Y. Lin, C.-S. Tang, V. Moldoveanu, J. H. Bardarson, and A. Manolescu, Phys. Rev. B **71**, 235302 (2005).
[23] J. H. Hsiao, K. M. Liu, S. Y. Hsu, and T. M. Hong, Phys. Rev. B **79**, 033304 (2009).